# Qualitative and Quantitative Assessments of Acid and Base Sites Exposed on Polycrystalline MgO Surfaces: Thermogravimetric, Calorimetric, and in-Situ FTIR Spectroscopic Study Combination

**G. A. H. Mekhemer,[†] S. A. Halawy,[‡] M. A. Mohamed,[‡] and M. I. Zaki*[,†]**

*Chemistry Department, Faculty of Science, Minia University, El-Minia 61519, Egypt, and Chemistry Department, Faculty of Science, South Valley University, Qena 83523, Egypt*

*Received: February 24, 2004; In Final Form: April 30, 2004*

Impact of the parent material used to yield magnesia on its surface properties was the prime objective of the present investigation. Accordingly, four test magnesias were obtained by calcination at 600 °C of four different parents: magnesium oxalate (to yield MgO−OX), carbonate (MgO−CA), hydroxide (MgO−HY), and perchlorate (MgO−PC). The surface accessibility was determined by $N_2$ sorptiometry at liquid nitrogen temperature, whereas the surface acid and base properties were assessed qualitatively and quantitatively by means of thermogravimetry, differential scanning calorimetry, and in-situ infrared spectroscopy of adsorption/desorption of pyridine and $CO_2$ at RT-400 °C. The reactivity of the surface acid and base sites thus revealed was gauged versus the decomposition of methylbutynol at 100 °C. The results obtained have shown the surface accessibility, basicity, and base site reactivity to assume the following descending order: MgO−OX > MgO−HY > MgO−CA > MgO−PC. Moreover, the results emphasize the importance of implementing the above-indicated combination of studies, if the nature, amount, and strength of surface acid and base sites are to be exhustively assessed

## Introduction

Research interest in assessing surface acid−base properties of metal oxides has been developing steadily with increasing dependence on the surface molecule model[1] in accounting for their adsorptive and catalytic behaviors. This is the more so since metal oxides have been increasingly sought in recent years to substitute for the less stable, though more active, noble metal catalysts in high-temperature total oxidation (combustion) processes.[2] Therefore, various methods have been devised to assess acid−base properties of metal oxide surfaces. These methods are classified as being either chemical,[3] thermochemical,[4] spectroscopic,[5−7] or catalytic[8] in nature. In conclusion, however, application of a combination of methods belonging to different classes has been considered much more informative and profitable than just leaning on different methods belonging to one-and-the-same class.[9] Recent reviews of results in the field[10−15] reveal the following general consensus: (i) the balance of research hitherto published is more tilted toward the surface acidity than the surface basicity, (ii) the amount of research using a combination of methods is much less than that employing individual methods, (iii) spectroscopic methods are more frequently used than the other methods, with infrared spectroscopy of adsorbed probe molecules being the most popular spectroscopic method adopted, and (iv) CO, $CO_2$, pyridine, and methylbutynol are the infrared probe molecules found to provide the widest range of information about structure, population, strength, and interactivity of acid and base sites on metal oxide surfaces.

In view of the above considerations, the present investigation was designed to assess the surface acid−base properties of polycrystalline magnesia, using a combination of desorption thermogravimetry, desorption calorimetry, and in-situ FTIR spectroscopy of adsorption and surface reactions of pyridine, $CO_2$, and methylbutynol. Frequency of the ring-breathing vibration modes ($\nu$CCN) of pyridine molecules is sensitive to both mode and strength of bonding to surface acid sites,[16] as well as to protonation. Thus, IR $\nu$CCN spectra (1700−1400 $cm^{-1}$) have been successfully used to examine availability and strength of various Lewis and Brønsted acid sites, as well as hydrogen-bond donor surface OH groups.[16] Moreover, the conversion of adsorbed pyridine molecules into α-pyridone or their breakdown into carboxylate, carbonate, and *N*-oxide species are considered indicative of the presence of reactive basic sites.[16] Analogously, end-on coordination and reactive adsorption of $CO_2$ molecules lead to IR $\nu$OCO spectra accounting for availability of Lewis acid and base sites, as well as surface $OH^{\delta-}$ groups.[17,18] On the other hand, surface reactions of methylbutynol molecules result in various pairs of products depending on the surface acid−base properties:[19,20] (i) acetone and acetylene are produced on basic surfaces, (ii) 3-methyl-3-buten-1-yne (MBYNE) and 3-methyl-2-buten-1-al (PRENAL) on acidic surfaces, and (iii) 3-hydroxy-3-methyl-2-butanone (HMB) and 3-methyl-3-buten-2-one (MIPK) on amphoteric surfaces.

The test polycrystalline magnesia (MgO) was obtained via four various precursor compounds, in hopes of having MgO crystallites of various sizes and, hence, surface areas and site coordination symmetries, densities, and acid−base properties.[21−24] MgO enjoys several important applications that are largely driven by its surface acid−base properties. The most prominent of these applications are two, namely, its application as a high-temperature adsorbent of $CO_2$ from gas streams in pressure-swing operations[25−27] and its use as an essential ingredient in the chemical makeup of deep oxidation catalysts.[28−30] Although

* Corresponding author. Fax: 002086360833; e-mail: mizaki@link.net.
[†] Minia University.
[‡] South Valley University.

10.1021/jp040164s CCC: $27.50 
Published on Web 08/10/2004

both types of applications are considered to be driven primarily by the strong surface basicity of MgO, stabilization of surface intermediates thus produced necessitates availability on the surface of Lewis acid sites.

## Experimental Section

**Test Magnesia Samples.** Four magnesia (MgO) samples were obtained via thermal decomposition at 600 °C for 4 h, in a dynamic atmosphere of air (50 $cm^3$/min), of four different parent materials: (i) MgO−PC was the product of magnesium perchlorate hexahydrate [$Mg(ClO_4)_2 \cdot 6H_2O$; 99.9% pure Aldrich product]; (ii) MgO−CA was the yield of basic magnesium carbonate [$Mg_5(CO_3)_4(OH)_2 \cdot 4H_2O$; AR-grade Prolabo product]; (iii) MgO−OX was the residue of a homemade magnesium oxalate dihydrate ($MgC_2O_4 \cdot 2H_2O$); and (iv) MgO−HY was the product of a laboratory-prepared magnesium hydroxide [$Mg(OH)_2$]. The decomposition temperature applied was chosen on basis of preliminary thermal analysis results of the parent materials. Authenticity of the chemical composition (MgO) and crystal structure (cubic unit cell) was verified by preliminary examinations, using infrared spectroscopy and X-ray powder diffractometry. All four oxide samples were similar in giving rise of three X-ray diffraction peaks at $2\theta = 10-70°$ corresponding almost identically to the standard *d* spacings (2.102 Å (100%), 1.483 Å (42.5%), and 2.447 Å (21.5%)) filed for cubic MgO in the JCPDS card no. 4-0829.[31] X-ray line broadening technique[32] was implemented with Scherrer's equation[32] to derive the following average crystallite sizes for the test oxide samples: 426 Å for MgO−PC, 142 Å for MgO−CA, 85 Å for MgO−HY, and 71 Å for MgO−OX.

The parent magnesium oxalate compound was prepared, adopting a similar procedure to that used previously to prepare copper oxalate,[33] by sprinkling of particles of the basic carbonate onto a 0.3 M aqueous solution of oxalic acid [$H_2C_2O_4 \cdot 2H_2O$; AR-grade Aldrich product] with continuous stirring and heating at 50 °C until effervescence of $CO_2$ was ceased. The white precipitate thus obtained (the oxalate compound) was left to settle at 50 °C for 12 h, filtered off, washed with distilled water, and heated at 100 °C till complete dryness (constant mass). On the other hand, the parent hydroxide was prepared by adding concurrently a 2 M aqueous solution of sodium hydroxide [NaOH; AR-grade Prolabo product] and 100 mL of hydrogen peroxide solution [$H_2O_2$; 30 wt % Merck product] to an aqueous solution (82.2 g/300 mL) of magnesium sulfate heptahydrate [$MgSO_4 \cdot 7H_2O$; AR-grade Prolabo product] till complete precipitation. The white precipitate (the hydroxide) thus yielded was filtered off, washed with distilled water until sulfate-freed, and dried at 110 °C.

BET-analysis[34] of $N_2$ adsorption data determined at liquid nitrogen temperature (−195 °C) found the test magnesia samples MgO−PC, MgO−CA, MgO−HY, and MgO−OX to assume, respectively, the following specific surface areas: 5, 45, 78, and 91 $m^2$/g. It is obvious that the surface area is inversely related to the crystallite size of the oxide (see above).

**Adsorptives and Gases.** Adsorptive molecules of pyridine (Py) and methylbutynol (MBOH) were provided by expanded vapors of pyridine [$C_5H_5N$; AR-grade Merck product] and methylbutynol [$(CH_3)_2C(OH)C{\equiv}CH$; AR-grade Merck product] liquids. Prior to application, the liquids were deaerated by on-line freeze−pump−thaw cycles performed at liquid nitrogen temperature. The source gas of adsorptive molecules of carbon dioxide ($CO_2$) was 99.99% pure Merck product, which was used as supplied.

Oxygen ($O_2$) and nitrogen ($N_2$) gases used to furnish the atmosphere for in-situ thermal pretreatments were 99% pure products of the Egyptian Company of Industrial Gases. Passing them through liquid nitrogen-cooled traps further purified them.

**Thermal Analyses.** Thermogravimetry (TG & DTG) and differential scanning calorimetry (DSC) were performed on small portions (10−15 mg) of test magnesia samples (before and after exposure to adsorptive atmospheres) while being heated (at 20 °C/min) in a dynamic $N_2$ gas atmosphere (50 $cm^3$/min), using a Shimadzu "stand alone" thermal analyzer equipped with a TGA-50H thermobalance, a DSC-50 microcalorimeter, and a TA-50WSI data acquisition and handling system. For DSC measurements, (i) highly sintered $\alpha$-$Al_2O_3$ powder (Shimadzu Corp.) was the thermally inert reference material used, and (ii) temperature and enthalpy readings were, respectively, calibrated versus the melting point (=156.3 °C)[35] and heat of fusion ($\Delta H_f$ = 28.24 J/g)[35] of Specpure Indium metal (a Johnson Matthey product).

Preexposure of test samples to $CO_2$ molecules was facilitated by placing small amounts (50−60 mg) of the samples, following heating them at 500 °C for 2 h in air, into an all-glass chamber fitted with gas inlet and outlet allowing for a stream of 100 $cm^3$ $CO_2$/min at RT. After the elapse of 2 h, small portions (10−15 mg) of the $CO_2$-covered samples were subjected to the above-described thermal analyses in $N_2$ atmosphere. On the other hand, Py-covered test samples were obtained following a 7-day exposure of small amounts of the samples (preheated at 500 °C) to pyridine vapor expanded into a preevacuated desiccator at RT. TG and DSC results of the adsorbed species were obtained following subtraction of results exhibited by corresponding test samples examined prior to exposure to adsorptive molecules.

**In-Situ Infrared Spectroscopy.** A Pyrex/Quartz glass cell equipped with $BaF_2$ windows, specially designed for high-temperature measurements,[36] was used to facilitate identifying products of the interactions of Py, $CO_2$, and MBOH molecules with surfaces of the test magnesia samples by in-situ Fourier transform infrared (FT-IR) spectroscopy in the transmission mode. A model Genesis-II FT-IR Mattson spectrometer was used for the measurements (averaged 100 scans at 2.0 $cm^{-1}$ resolution), and installed WinFIRST Lite v1.02 software was the means whereby spectra acquisition and processing were carried out. Thin (20−30 mg/$cm^2$), but coherent, self-supporting wafers of test samples were mounted inside the cell, activated in a stream of $O_2$ (50 $cm^3$/min) at 450 °C for 1 h, and, subsequently, outgassed at the same temperature and $10^{-5}$ Torr for 30 min. The temperature was, then, decreased to RT under dynamic vacuum, the wafer and cell background spectra were acquired, and a certain dose (0.5−20 Torr) of Py, $CO_2$, or MBOH gas phase was admitted into the cell. The gas/solid interface was maintained at RT for 5 min prior to (i) recording a spectrum of the gas phase (+cell background), (ii) recording a spectrum of the solid phase (+gas phase, cell background and adsorbed species), (iii) pumping off the gas phase for 5 min, and (iv) measuring a spectrum of the solid phase (+adsorbed species and cell background). This sequence of measurements was repeated at higher temperatures (100−400 °C), and the spectra were measured after cooling to RT. Difference spectra of gas phase and adsorbed species were obtained by absorption subtraction of the cell and wafer background spectra, using the installed software.

## Results and Discussion

**Nature of Surface Acid and Base Sites.** Figure 1 compares IR spectra taken at 1700−1400 $cm^{-1}$ of Py adsorbed on the test magnesias at RT, with those taken following 5-min

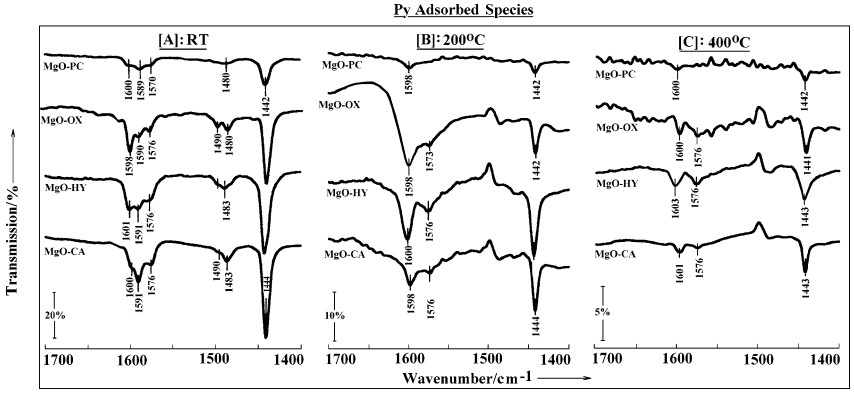


**Figure 1.** IR $\nu$CCN spectra of pyridine (Py)-adsorbed species established on the various test magnesias following thermoevacution at $10^{-5}$ Torr and the temperatures indicated for 5 min.

**TABLE 1: Desorption Thermogravimetry and Calorimetry of Room-Temperature Adsorbed Pyridine (Py) and $CO_2$ Molecules on the Test Magnesias**

| | | Py | | | | | | $CO_2$ | | | | | |
|---|---|---|---|---|---|---|---|---|---|---|---|---|---|
| MgO | | adsorbed[a] | | desorbed | | | | adsorbed[a] | | desorbed | | | |
| sample | $S_{BET}$ ($\pm$2m$^2$/g) | ($\pm$1 mg/g) | (molc/100 Å$^2$)[b] | $T_d$(max)/°C[c] | ($\pm$1 mg/g) | (molc/100 Å$^2$)[b] | $\Delta H^d$ (kJ/mol) | ($\pm$1 mg/g) | (molc/100 Å$^2$)[b] | $T_d$(max)/°C[c] | ($\pm$1 mg/g) | (molc/100 Å$^2$)[b] | $\Delta H^d$ (kJ/mol) |
| MgO−OX | 91 | 309.0 | 26 | 68 & 130 | 272.7 | 23 | 12.0 | 154. 0 | 23 | 121 | 75.0 | 11 | 132.0 |
| | | | | 324 | 36.3 | 3 | 72.9 | | | 354 | 79.0 | 12 | 80.7 |
| MgO−HY | 78 | 106.6 | 11 | 51 & 117 | 75.6 | 8 | 29.2 | 121. 6 | 22 | 125 | 70.0 | 12 | 114.6 |
| | | | | 338 | 31.0 | 3 | 69.5 | | | 379 | 51.6 | 10 | 56.1 |
| MgO−CA | 45 | 53.3 | 9 | 123 | 33.3 | 5 | 147. 1 | 80.3 | 25 | 117 | 41.4 | 12 | 78.0 |
| | | | | 333 | 20.0 | 3 | 222. 4 | | | 354 | 38.9 | 12 | 42.6 |
| MgO−PC[e] | 5 | $3.0 \times 10^{-3}$ | $4.5 \times 10^{-3}$ | 120 | $3.0 \times 10^{-3}$ | $4.6 \times 10^{-3}$ | 24.2 | 5.3 | 15 | 120 | 5.3 | 15 | 16.2 |

[a] At room temperature. [b] Number of molecules per 100 Å$^2$, approximated to the nearest figure. [c] As resolved in a corresponding DTG curve. [d] Calculated following subtraction of observed contributions of the adsorbent. [e] MgO−PC exhibited very weak and ill-defined features in the TG and DSC curves; therefore, the calculated data must not be given much credit.

thermoevacuation at 200° and 400 °C. Irreversibly adsorbed Py molecules at RT (Figure 1A) exhibit similarly four absorptions due to the normal modes 8a (1591−1589 cm$^{-1}$), 8b (1576−1570 cm$^{-1}$), 19a (1483−1480 cm$^{-1}$), and 19b (1444−1442 cm$^{-1}$) of the ring-breathing ($\nu$CCN) vibrations.[16] The parallel intensification observed for the 8a and 19b bands, going from the spectrum of MgO−OX down to that of MgO−CA in Figure 1A, may be considered indicative of a gradual development of Py−Py intermolecular interactions or, in other words, a gradual transition from a gas-like (loose) to a liquid-like (compact) adsorbed layer.[37] As a matter of fact, the twin-bands displayed at 1490 and 1480 cm$^{-1}$ in the spectrum taken of Py/MgO−OX at RT are actually P and R branching of the 19b absorption, thus indicating freely rotating Py molecules in a gaslike adsorbed layer.[37]Accordingly, such reorganization of the adsorbed layer may impart an enhanced accumulation of physisorbed molecules (PPy) as the adsorbing surface becoming more and more flatter and extended. The fact that the specific surface area decreases correspondingly (see Table 1, above) is rather supportive. On the other hand, the high-frequency shift experienced by the 8a band, leading eventually to a band at 1601−1598 cm$^{-1}$ on all test samples, is assignable to Py molecules coordinated to Lewis acid sites (LPy).[16]

Following a brief thermoevacuation at 200 °C, the spectra obtained (Figure 1B) help making the following observations: (i) the complete disappearance of bands assignable to PPy molecules and (ii) a considerable weakening of bands (at 1600−1598 cm$^{-1}$) assignable to LPy molecules, most obviously on MgO−PC and MgO−CA (cf. the change in the transmission scale). The weakening of LPy bands is furthered upon a further increase of the thermoevacuation temperature to 400 °C (Figure 1C), leaving behind nothing but minute amounts of Py molecules anchored on Lewis acid sites. Low-temperature IR carbonyl spectra taken by Ulla et al.[30] of CO/MgO revealed the availability of two different Lewis acid sites on the magnesia surfaces: five-fold ($Mg^{2+}_{5f}$) and four-fold ($Mg^{2+}_{4f}$) coordinated magnesium ions. Also, none of the IR diagnostic absorptions of α-pyridone ($\nu$C═O at 1580−1560 cm$^{-1}$)[16] and pyridinium oxide ($\nu$N$^+$−O at 1260−1250 cm$^{-1}$) species have been detectable in the spectra obtained at ≥200 °C. Hence, one may safely presume that the high-temperature desorbing species from Py/MgO are intact Py molecules, for the Lewis acid sites are not sufficiently strong to activate Py ligands for a synergic surface oxidation.

To assess the nature of the surface base sites exposed on the test magnesias, IR spectra were taken of adsorbed $CO_2$ molecules as a function of the gas pressure at RT and as a function of thermoevacuation temperature. The set of $\nu$OCO spectra exhibited in Figure 2A are typical for $CO_2$ adsorbed on MgO−CA, MgO−OX, and MgO−HY. At RT, the spectra obtained following exposure to 0.5 Torr of $CO_2$ monitor two strong broad bands centered arround 1515 and 1403 cm$^{-1}$, due respectively to $\nu_{as}$OCO and $\nu_s$OCO vibrations of monodentate-bound carbonate species ($\Delta\nu = \nu_{as} - \nu_s < 200$ cm$^{-1}$).[18] They monitor, moreover, two largely overlapping weaker bands occurring at the higher frequencies of 1684 and 1646 cm$^{-1}$, which are assignable to $\nu_{as}$OCO vibrations. Such high-frequency antisymmetric stretching vibrations of OCO bonds are usually considered for bidentate carbonate or bicarbonate species.[18] The corresponding symmetric stretching vibrations should occur, respectively, at 1350−1270 and 1450−1400 cm$^{-1}$, that is, they may still contribute to the large absorption centered around 1403 cm$^{-1}$. Upon increasing the $CO_2$ gas pressure gradually up to 20 Torr, the initial bands grew concomitantly stronger with the

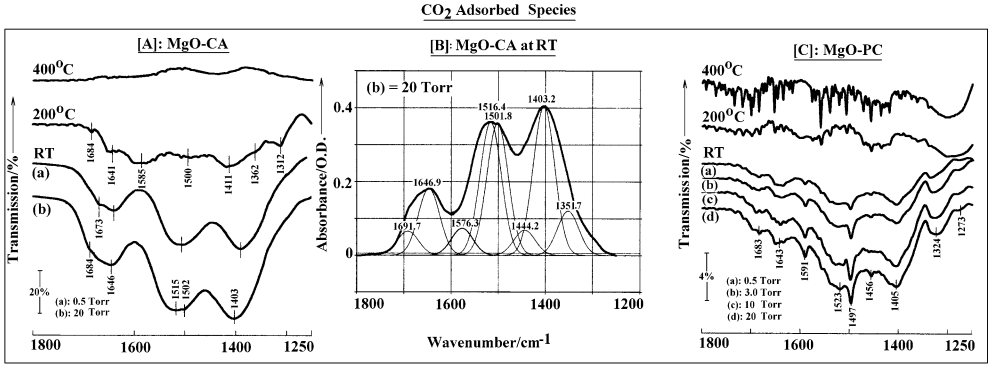


**Figure 2.** IR $\nu$OCO spectra of $CO_2$-adsorbed species established on MgO−CA [A] and MgO−PC [C] as a function of the gas pressure at RT and following thermoevacution at $10^{-5}$ Torr and the temperatures indicated for 5 min. [B] Deconvolution results of $\nu$OCO absorption bands observed following exposure of MgO−CA to 20 Torr $CO_2$ at RT.

emergence of an ill-defined maximum at 1505 $cm^{-1}$ (Figure 2A).

When the bands observed in the latter spectrum (20 Torr) were deconvoluted by means of standard PeakFit software, eight absorption contributions were resolved (Figure 2B). Frequencies of the resolved absorptions are rather close to those observed in the well-resolved spectra taken of RT-adsorbed $CO_2$ on the low-surface area MgO−PC (Figure 2C) or on the other high-area magnesias at >RT (Figure 2A). The absorptions resolved in these spectra may account for two different monodentate carbonate species: type-I, exhibiting absorptions at 1523−1516 ($\nu_{as}$OCO) and 1456−1444 $cm^{-1}$ ($\nu_s$OCO), and type-II, giving rise to absorptions at 1501−1497 ($\nu_{as}$OCO) and 1405−1403 $cm^{-1}$($\nu_s$OCO).[18,27] These resolved absorptions help revealing that the high-frequency $\nu_{as}$ vibrations observed at >1600 $cm^{-1}$ may indeed be due to bidentate carbonate species (1691−1683 ($\nu_{as}$OCO) and 1362−1324 $cm^{-1}$ ($\nu_s$OCO)) and bicarbonate species (1646 ($\nu_{as}$OCO), 1405 ($\nu_s$OCO), and 1225 $cm^{-1}$ ($\delta$HOC)).[18,27] The absorptions at 1591−1585 $cm^{-1}$ could well be due to $\nu_{as}$OCO vibrations of another type of bidentate carbonate species, whose $\nu_s$OCO vibrations would be responsible for the absorption at 1312−1273 $cm^{-1}$.[18] It is worth noting, however, that (i) absorptions assigned to bicarbonate species were relatively more obvious on MgO−OX and MgO−HY, and hardly accessible on MgO−PC, (ii) the expected $\nu$HO absorption of bicarbonate species was ill-defined on all test magnesias which may, conversely, throw shadows of doubt on the bicarbonate formation, and (iii) no absorptions were observed at 2400−2200 $cm^{-1}$, thus indicating the absence of physisorbed and end-on chemisorbed $CO_2$ molecules.[18] In a preliminary examination, bulk $MgCO_3$ had given rise to an IR spectrum displaying sharp $\nu$OCO absorptions at 1521, 1491, and 1424 $cm^{-1}$. Accordingly, the sharp absorptions (namely, at 1591, 1523, 1497, and 1456 $cm^{-1}$) monitored in the spectra displayed in Figure 2C may, presumably, be assigned to bulklike carbonate species.[38]

Following a brief thermoevacuation at 200 °C, the spectra taken of $CO_2$/MgO (Figure 2A and 2C) monitor much weaker absorptions due, mainly, to bidentate and bulklike carbonate species. Upon a further increase of the thermoevacuation temperature up to 400 °C, the spectra observed hardly monitor absorptions due to surface or bulk carbonates. Hence, one may conclude that surface monodentate carbonate and bicarbonate species (if any) are thermally less stable than both the bidentate and bulklike carbonate species. Similar conclusions have been drawn earlier.[18,27,39]

Accordingly, IR spectra taken of adsorbed Py or $CO_2$ molecules on the test magnesias may help characterizing the

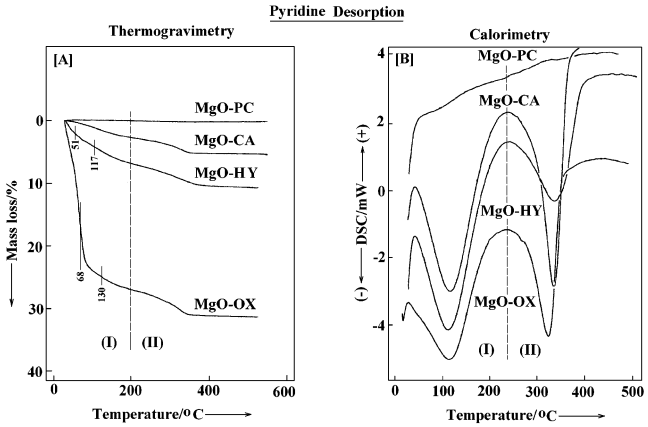


**Figure 3.** Pyridine desorption thermogravimetry [A] and differential scanning calorimetry [B] on the magnesias indicated.

presence of Lewis acid sites (cus $Mg^{2+}{}_{4f}$ or $Mg^{2+}{}_{5f}$). These sites are capable of stabilizing formation of presumably two different types of monodentate and bidentate carbonate species, but are too weak to coordinate $CO_2$ molecules and, hence, facilitate its interaction with nearby surface $OH^-$ groups to give rise to stable bicarbonate species. As a matter of fact, many earlier reports have excluded formation of bicarbonate species on magnesia surfaces.[18,38] Strong and medium-strong base sites (cus $O^{2-}$, $O^-$, or $OH^-$ sites) are most likely available on the examined surfaces; in the meantime, the absence of Brønsted acid sites (proton-donor sites) is evident on all the test surfaces. Spectral indications for formation of bulklike carbonate species, as has been suggested earlier by Gregg and Ramsay,[38] may account for bulk incursions of adsorbed $CO_2$ species.

**Amount and Strength of Acid and Base Sites.** Figure 3 exhibits Py desorption TG curves (3A) as well as the corresponding DSC curves (3B). The TG curves monitor two mass loss (desorption) steps (I and II), except for Py/MgO−PC where mass loss is hardly detectable. Consistently, the DSC curves (desorption calorimetry) monitor two endotherms. Differential analysis (DTG) of the mass loss steps showed step-I (at <200 °C) of Py/MgO−OX and Py/MgO−CA to consist of two strongly overlapping desorption processes. Compatibly, the corresponding endotherm (I) is considerably broader than the following one (endotherm-II). Temperatures at which the rate of the various mass loss and enthalpy changes are maximized ($T_d$(max)) are given in Table 1. Table 1 also sets out the specific surface area ($S_{BET}$/$m^2g^{-1}$) of the test adsorbents and the specific (mg/g) and intrinsic (molecule/100 $A^2$) amounts of Py adsorbed at RT. Moreover, specific and intrinsic amounts of Py desorbed in correspondence to the various $T_d$(max) values, as well as the

DSC-derived molar enthalpy change ($\Delta H$/kJ mol$^{-1}$) corresponding to each desorption step, are given in Table 1.

It is obvious from the TG and DSC data given for Py/MgO in Table 1 that both the specific and intrinsic amounts of adsorbed Py at RT change in conform to the change in the specific surface area of the adsorbent. Because the cross-sectional area of a perpendicularly bound Py molecule occurs in the range of 28−33 Å,[2,40] a compact monolayer would have ca. 3 Py molecules per 100 Å$^2$ of the surface. If we exclude the data given for MgO−PC for obvious uncertainty, the observed decrease of the intrinsic amount of adsorption (26 → 9 molecules/100 Å$^2$) with the surface area (91→ 45 m$^2$/g) would mark a gradual retrogression of multilayer (weak) adsorption, thus emphasizing the importance of the surface chemistry. This can be easily confirmed by the desorption data, where the amount of Py molecules in excess of the monolayer capacity (ca. 3 Py/100 Å$^2$) is desorbed via the mass loss step-I (Figure 3A) occurring at <200 °C. Independent of the adsorbent nature, the retained amount of Py molecules (chemisorbed) to be desorbed through step-II (at >200 °C) is invariably equal to the monolayer capacity.

Recalling the IR results of adsorbed Py as a function of temperature (Figure 1), Py molecules desorbed at 200 °C (i.e., throughout the first step (I) of desorption) are essentially physisorbed molecules. The observed increase in the corresponding enthalpy change from 12 (MgO−OX) to 29.2 (MgO−HY) and further to 147.1 kJ/mol (MgO−CA) may account for a corresponding increase in the contribution of relatively more strongly bound molecules to the overall amount of physisorbed Py. Indeed, the IR spectra obtained for RT-adsorbed Py monitored a transition from gaslike to liquidlike adsorbed layers going from MgO−OX to MgO−HY and, further, to MgO−CA (Figure 1A). The reported range of enthalpy of physisorption of Py on metal oxide surfaces lies below 60 kJ/mol.[4] Thus, the considerably higher enthalpy change (147.1 kJ/mol) observed for Py/MgO−CA desorbed through step-I may be considered indicative of the removal of molecules exchanging a stronger mode of bonding with the surface (e.g., hydrogen bonding). Admittedly, however, it is neither possible to confirm formation of hydrogen-bonded Py molecules nor to exclude it with certainty from the IR spectra in hand (Figure 1A).

On the other hand, the enthalpy of chemisorption of Py (i.e., Py coordinated to Lewis acid sites), as determined previously using differential calorimetry, lies in the range 80−230 kJ/mol.[4,41] Accordingly, the varied enthalpy change (69.5−222.4 kJ/mol) determined for Py desorption throughout step-I, which occurs at the expense of purely chemisorbed Py on Lewis acid sites (Figure 1), may well be considered to gauge the strength of the Lewis acid sites involved. Hence, the Lewis sites involved in chemisorbing Py on MgO−OX ($\Delta H$ = 72.9 kJ/mol) or MgO−HY ($\Delta H$ = 69.5 kJ/ mol) are of comparable strength, which is much less than the strength of Lewis sites chemisorbing Py on MgO−CA ($\Delta H$ = 222.4 kJ/mol).

Figure 4 displays TG (4A) and DSC curves (4B) of desorption of RT-adsorbed $CO_2$ on the test magnesias. The mass loss and $\Delta H$ data therefrom derived are compared in Table 1. Here also, the TG and DSC curves monitor two desorption steps (I and II) of adsorbed $CO_2$. The DSC curves show apparently that step-I involves two strongly overlapping desorption processes, as well as an intermediate, weak endotherm near 260 °C. The comparison held in Figure 5 between the DSC curves of MgO−OX before and after exposure to $CO_2$ molecules reveals that the composite nature of the endotherm corresponding to step-I and the intermediate endotherm near 260 °C are due largely to

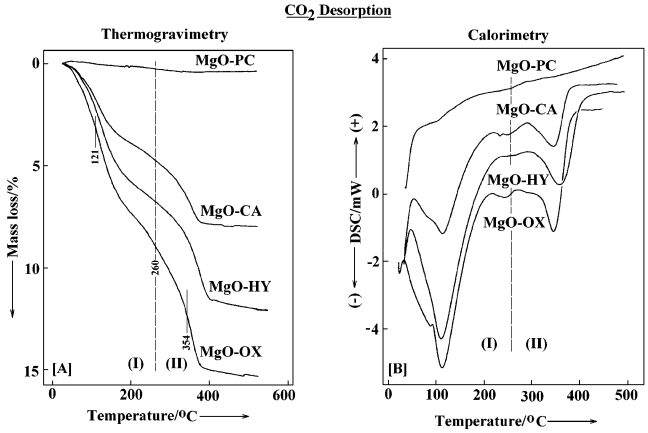


**Figure 4.** $CO_2$ desorption thermogravimetry [A] and differential scanning calorimetry [B] on the magnesias indicated.

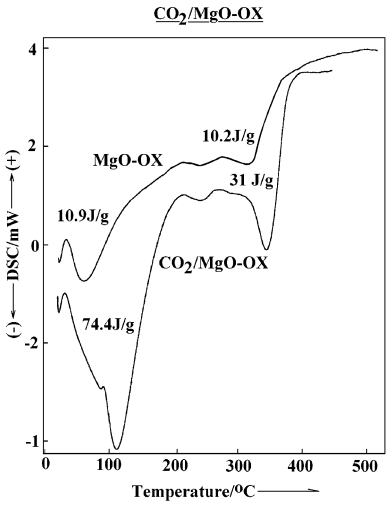


**Figure 5.** Differential scanning calorimetry curves obtained for MgO−OX before and after $CO_2$ adsorption at RT.

contributions from the adsorbent. This observation has been found applicable to the other adsorbents. Accordingly, the enthalpy changes reported in Table 1 have been obtained following subtraction of the adsorbent contributions.

Similarly to the case of adsorbed Py, the specific amounts of RT-adsorbed $CO_2$ are shown (Table 1) to change in conform to the change of the specific surface area of the test magnesias. In contrast, however, the intrinsic amounts of adsorbed $CO_2$ assume almost a constant value (ca. 23 ± 1 molecules/100 Å$^2$), overlooking that determined for MgO−PC for uncertainty. This result may account in contrast to Py adsorption that one-and-the-same types of $CO_2$ adsorption occur irrespective of the sample of test magnesia. Considering the cross-sectional area of $CO_2$ (18−20 Å$^2$/molecule),[38] the monolayer capacity of the surface should not exceed ca. 5 molecules/100 Å$^2$. Accordingly, the amount in excess of the monolayer capacity might be due to a multilayer type of adsorption or bulk absorption of $CO_2$ molecules. The fact that IR results of $CO_2$ adsorption on the various magnesias (Figure 2) do not account for occurrence of physisorption may attribute the extra monolayer amounts to $CO_2$ absorption. The detection of IR $\nu$OCO absorptions having similar frequencies to those of bulklike carbonate species may lend a further support to this suggestion.

Overlooking the data derived for MgO−PC, the intrinsic amounts of desorbed $CO_2$ molecules through the first (I) and second (II) mass loss steps assume almost a constant value (11 ± 1 molecules/100 Å$^2$), which is almost twice as much as the

monolayer capacity of $CO_2$ adsorption. If MgO(100) were the crystal facet predominantly exposed at the surface of polycrystalline magnesia, as prophesied by many interested researchers,[22,38,42] then the surface site densities of the metal and oxide sites would be equally 11.3 $Mg^{2+}$ or $O^{2-}$/100 Å$^2$.[38] Consequently, the saturation coverage of $CO_2$/MgO (ca. 5 molecules/100 Å$^2$) would correspond to formation of a bidentate carbonate species (i.e., $CO_2$/2.2 $Mg^{2+}$ or $CO_2$/2.2 $O^{2-}$). On the basis of the IR results (Figure 2A and 2C), most of the $CO_2$ molecules desorbed throughout step-I should be released mainly by monodentate carbonate species, whereas those desorbed via step-II would be released by bidentate and bulklike carbonate species. As result, one may attribute the extra monolayer amounts of $CO_2$ determined via step-II to bulklike carbonate species. The fact that bulk $MgCO_3$ is thermally stable to temperatures well above the $T_d$(max) of step-II (=354−379 °C), namely, ≥430 °C, it is plausible to attribute bulklike carbonates to ionic carbonates accommodated into the surface layer, rather than to carbonates deeply rooted in the bulk.

An inspection of the enthalpy changes corresponding to step-I and -II reveals that the higher values are assumed by step-I ($\Delta H$ = 132.0−78.0 kJ/mol vs 80.7−42.6 kJ/mol for step-II) and that both step-I and -II enthalpy changes decrease with the specific surface area of the adsorbent. Since the surface acidity does not play the determining role in the formation of surface carbonate species, it is, therefore, the basicity of the surface that is gauged by the derived enthalpy changes. Thus, the fact that stronger base sites are involved in the formation of monodentate carbonates (i.e., those decomposing essentially throughout step-I) may explain the higher $\Delta H$ values derived for step-I desorption. On the other hand, the overall decrease of $\Delta H$ values of step-I and -II with the surface area may, thus, be attributed to elimination of base sites of distinct $CO_2$ adsorption activity, such as corner, edge, and defect sites, as the specific area decreases and the surface becomes flatter and more extended.

In conclusion, the results given in Table 1 would underline MgO−OX as the magnesia having the strongest base sites and MgO−CA as that having the weakest (excluding MgO−PC). TPD results of the influence of heating gas atmosphere on the basicity of MgO powders[43] have observed three $CO_2$ desorption peaks at 150, 260, and 370 °C and have found that the inert atmosphere of He helps generation of stronger base sites more than the oxidizing atmospheres of air or oxygen. Moreover, Auroux and Gervasini,[44,45] using differential microcalorimetry, have compatibly determined an overall enthalpy change of 120−130 kJ/mol for $CO_2$ adsorption on high-area MgO at RT.

**Reactivity of Surface Base Sites.** The known specificity of the decomposition of methylbutynol (MBOH) (into acetone and acetylene) to the availability on the catalytic surface of strong basic sites[19,20,46] has been exploited to test the reactivity of base sites on the present test magnesias. Therefore, in-situ IR spectroscopy was applied to examine the adsorption and surface reactions on the test magnesias as a function of temperature (RT-200 °C). Figure 6A demonstrates gas-phase spectra taken of MBOH/MgO−CA at RT, 100 °C, and 200 °C, which are typical of the gas-phase spectra taken of MBOH ($(CH_3)_2C(OH)$−C≡CH) over all of the test magnesia. The spectrum obtained at RT monitors nothing but the diagnostic absorptions of the $\nu$OH (3645 cm$^{-1}$), $\nu$HC≡ (3329 cm$^{-1}$), $\nu$CH (2996, 2947, and 2887 cm$^{-1}$), $\nu$C≡C (2124 cm$^{-1}$), $\delta$CH (1458, 1370, and 1327 cm$^{-1}$), $\delta$OH (1261 cm$^{-1}$), $\nu$CO (1180 cm$^{-1}$), and $\nu$C−C (1125 cm$^{-1}$) vibrations of pure MBOH molecules.[19,20] The very weak absorption at 2070 cm$^{-1}$ is an overtone. At 100 °C, the spectrum

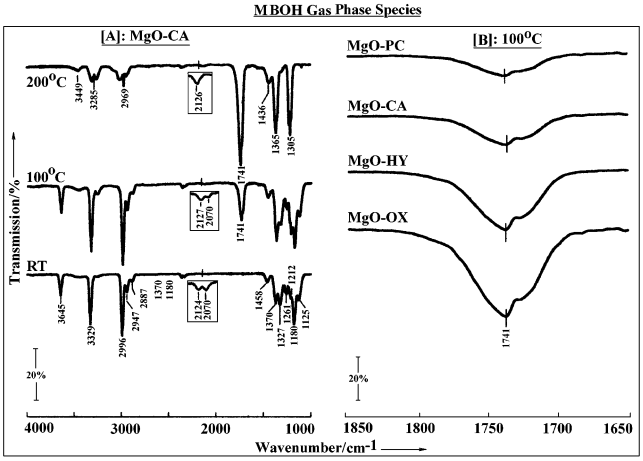


**Figure 6.** IR spectra taken of MBOH gas phase over MgO−CA at the temperatures indicated [A], and over the test magnesias indicated at 100 °C [B].

indicates slight, general weakening of the alcohol absorptions, with the emergence of a sharp absorption of $\nu$C=O vibrations (at 1741 cm$^{-1}$) of acetone molecules.[19,20] At 200 °C, the spectrum declares complete disappearance of the alcohol molecules. Instead, it displays strong absorptions (at 2969, 1741, 1436, 1365, and 1305 cm$^{-1}$) due to various vibrations of acetone molecules,[47] as well as weak absorptions due to $\nu$HC≡ (3285 cm$^{-1}$) and $\nu$C≡C (2126 cm$^{-1}$) vibrations of free acetylene molecules.[19] These results indicate that MBOH molecules are only partially decomposed at 100 °C and completely decomposed into acetone and acetylene molecules at 200 °C over MgO−CA. Therefore, Figure 6B compares the absorptions observed at 100 °C for $\nu$C=O of acetone molecules formed over the various test magnesias to gauge the extent of decomposition of the alcohol, and hence the surface basicity. The % decomposition, calculated by relating the integrated absorbances derived from Figure 6B to that of the maximal absorbance assumed by the $\nu$C=O vibrations at 200 °C (Figure 6A), is ca. 30% over MgO−PC, 36% over MgO−CA, 67% over MgO−HY, and 91% over MgO−OX at 100 °C. Because almost identical amounts (30 ± 1 mg) were used of the various test magnesias, the same amount of MBOH vapor (10 Torr) was admitted into the reactor/cell, and the gas-phase spectra were taken under almost identical spectroscopic conditions, the % decomposition established may help rank the surface basicity of the test magnesias in the following descending order: MgO−OX > MgO−HY > MgO−CA > MgO−PC. However, to credit this ranking, and to compare it with the above presented and discussed TG and DSC results, one has to find out whether the amounts of acetone molecules released into the gas phase are the absolute decomposition product or equilibrium amounts of a subsequent involvement of acetone molecules into surface polymerization (aldol-condensation-type) reactions.[47]

Figure 7 exhibits IR spectra taken of MBOH adsorbed species on MgO−CA as a function of temperature; background spectra of the adsorbent (i.e., those recorded before exposure to the alcohol vapor) are given for comparison purposes. The spectra recorded at RT clearly show absorption bands of the various vibrational modes of adsorbed MBOH to be shifted relative to those of the free molecule (Figure 6A). Thus, the $\nu$HC≡ vibrations appear at 3321−3274 cm$^{-1}$, and the $\nu$CH vibrations of the methyl groups appear at 2983−2874 cm$^{-1}$ (Figure 7A). On the other hand, absorption bands due to $\delta$CH/$\nu$C−O/$\nu$C−C vibrations are displayed at 1462−1124 cm$^{-1}$ (Figure 7B). According to Hasan et al.,[20] these latter absorptions are

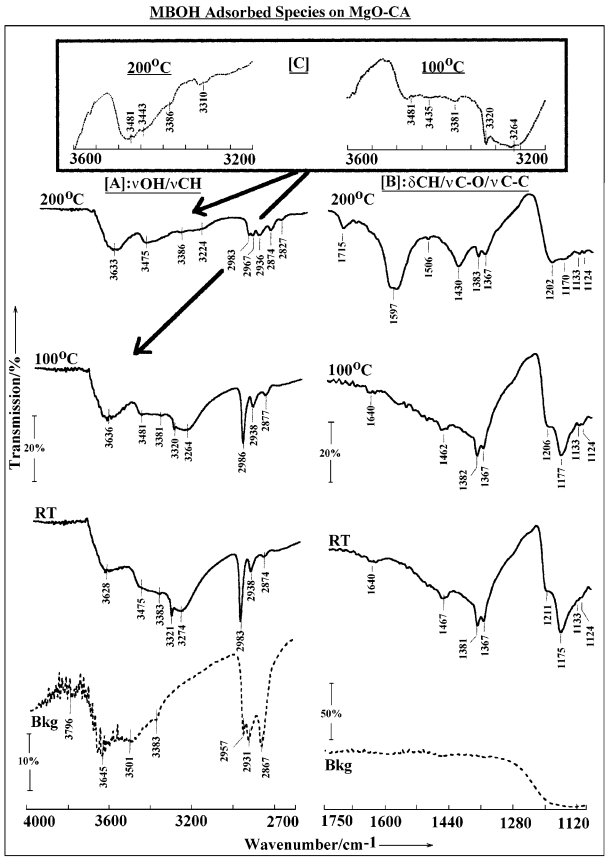


**Figure 7.** IR $\nu$OH/$\nu$CH [A] and $\delta$CH/$\nu$C−O/$\nu$C−C [B] spectra of MBOH adsorbed species established on MgO−CA following thermoevacuation at the temperatures indicated for 5 min. [C] Insets: close-ups at the spectra obtained at the temperatures indicated over the frequency range 3600−3200 $cm^{-1}$.

assignable to dissociative adsorption of MBOH molecules on acid−base ($M^{n+}-O^{2-}$) pair sites to form alkoxide species (methylbutynoxide, $MBO^-$) as depicted in the following reaction:

$$MBOH + M^{n+}(s) + O^{2-}(s) \rightarrow MBO^- \cdots M^{n+}(s) + HO^-(s) \quad (1)$$

where (s) denotes "surface", and $MBO^-$ is the $(CH_3)_2C(O^-)C\equiv$CH species.

In this process, a strongly basic ($O^{2-}$) site is required to abstract the hydrogen atom from the alcoholic OH, and, simultaneously, the resulting alkoxide group is anchored to the Lewis acid ($M^{n+}$) site to form the alcoholate species.[20] It has also been reported[19] that MBOH molecules have two H-bonding centers, namely, the alcoholic OH and the acetylenic group. H-bonding involving the alcoholic OH may also lead to the formation of alkoxide species, as suggested by the following reaction:

$$MBOH + M^{n+}(s) + HO^-(s) \rightarrow MBO^- \cdots M^{n+}(s) + H_2O\uparrow \quad (2)$$

The occurrence of this reaction does not require the strong basicity demanded by the preceding one (eq 1). On the other hand, Fouad et al.[19] have suggested two modes of adsorptive interactions of MBOH molecules involving the acetylenic group: (i) an interaction with strong Lewis base sites involving the acetylenic hydrogen ($\equiv C-H\cdots O^{2-}(s)$) and (ii) an interaction with Lewis acid sites involving the $\pi$-electrons. These authors have found the former mode of interaction to cause a greater red shift of the $\nu$HC≡ frequency than the latter one. The present spectra (Figure 7A) display two $\nu$HC≡ absorptions at RT (at 3321 and 3274 $cm^{-1}$). Accordingly, the low-frequency absorption (3274 $cm^{-1}$) makes a much larger red shift ($\Delta\nu$ = 3329−3274 = 55 $cm^{-1}$) than the high-frequency absorption ($\Delta\nu$ = 8 $cm^{-1}$). This may indicate that MgO−CA exposes strong base sites ($O^{2-}$) capable of bonding the acetylenic hydrogen and Lewis acid sites weakly interacting with the acetylenic $\pi$-electrons.

The above-characterized MBOH adsorbed species at RT appear to remain stable to heating at 100 °C. The spectra obtained at 100 °C (Figure 7A and 7B) bear a great deal of resemblance to those obtained at RT, except for a further red shift of the low-frequency $\nu$HC≡ absorption to 3264 $cm^{-1}$ (see inset C). At 200 °C, however, the spectra obtained reveal some radical spectral changes: (i) appreciable weakening of absorptions in the $\nu$OH/$\nu$CH frequency region (Figure 7A), with the emergence of two new $\nu$CH absorptions at 2967 and 2827 $cm^{-1}$, (ii) considerable weakening of absorptions (in the $\delta$CH/$\nu$C−O/$\nu$C−C region) due to the alkoxide species, with the emergence of a strong, broad absorption centered around 1597 $cm^{-1}$, a medium absorption at 1430 $cm^{-1}$, and two weak, but distinct, absorptions at 1715 and 1506 $cm^{-1}$. The absorption at 1715 $cm^{-1}$ is most likely due to $\nu$C═O vibrations of acetone molecules coordinated to Lewis acid sites on the surface.[47] Acetone molecules have, indeed, been released into the gas phase via the decomposition of MBOH at 100−200 °C. However, its anchorage to the surface at >100 °C may mean that its chemisorption is an activation process. Accordingly, one may attribute the simultaneously emerging other absorptions (1597−1430 $cm^{-1}$) to adsorbed species that have been given rise by acetone further surface reactions.[47]

According to the results reported by Zaki et al.,[48] the 1597 $cm^{-1}$ absorption is assignable to $\nu$C═O vibrations of unsaturated carbonyl species (DAA or MSO), and the 1506 and 1430 $cm^{-1}$ absorptions are due, respectively, to relevant $\nu$C−C−O$^-$/$\nu$C═C and $\delta CH_2CO$ moieties. Similar spectral features were observed for MBOH adsorption on the other test magnesias. Thus, the IR spectra taken of MBOH on MgO−CA (Figures 6 and 7), as well as the other magnesias, at RT-200 °C may help making the following conclusive remarks: (i) acetone nondissociative chemisorption is an activated process, requiring temperatures >100 °C, (ii) chemisorbed acetone is the precursor for its condensation reactions, (iii) base sites available on the adsorbent are strong enough to facilitate the acetone further reactions, and (iv) amounts of acetone released into the gas phase of MBOH at 100 °C over all of the test magnesias are not involved in adsorption or further surface reactions at the temperature applied; thus, their quantitation can be considered a trustworthy gauge for the surface basicity.

## Conclusions

The above presented and discussed results may help emphasizing the dependence of not only the magnesia surface accessibility (specific surface area) on the parent material used to synthesize it but also the surface acid and base properties. The gravimetric, calorimetric, and infrared spectroscopic studies performed on pyridine, $CO_2$, and methylbutynol adsorption and surface reactions provided integrating information, whereby the surface accessibility, basicity, and base site reactivity assume the following descending order: MgO−OX > MgO−HY > MgO−CA > MgO−PC. As regards the surface acidity, the following descending order has been observed: MgO−CA ≫

MgO−OX ≈ MgO−HY > MgO−PC. The fact that the sole detectable decomposition course of methylbutynol on the test magnesias has been that yielding acetone and acetylene emphasizes, by virtue of the mechanistic attributes of the reaction,[49] an overwhelming basic nature for magnesia.

According to results of surface structural studies of polycrystalline MgO reported by Knözinger[22] and Zecchina et al.,[50] and the model surfaces presented by Farragher,[42] highly dispersed oxide particles expose highly irregular and defective surfaces whose properties may be dominated by some particularly energetic and reactive minority sites (e.g., edge, corner, and defect sites). Hence, the observed decrease of enthalpy of $CO_2$ chemisorption (Table 1) with the surface area of MgO may ascribe the above indicated descending order of the surface basicity to elimination of such distinctly basic sites as the surface becomes flatter and more extended.

**Acknowledgment.** M.I.Z. thanks with appreciation an equipment donation (V-8151/03042) by the Alexander von Humboldt Foundation (Bonn, Germany) that made possible a rehabilitation of the IR-reactor/cells used in the present work.

## References and Notes

(1) Davis, B. H. In *Handbook of Heterogeneous Catalysis*; Ertl, G., Knözinger, H., Weitkamp, J., Eds.; Wiley-VCH: Weinheim, 1997; vol. 1, pp 13−35.
(2) Garten, R. L.; Dalla Betta, R. A.; Schlatter, J. C. In *Handbook of Heterogeneous Catalysis*; Ertl, G., Knözinger, H., Weitkamp, J., Eds.; Wiley-VCH: Weinheim, 1997; Vol. 4, pp 1668−1677.
(3) Hall, K. W. In *Handbook of Heterogeneous Catalysis*; Ertl, G., Knözinger, H., Weitkamp, J., Eds.; Wiley-VCH: Weinheim, 1997; Vol. 2, pp 692−698.
(4) Spiewak, B. E.; Cortright, R. D.; Dumesik, J. A. In *Handbook of Heterogeneous Catalysis*; Ertl, G., Knözinger, H., Weitkamp, J., Eds.; Wiley-VCH: Weinheim, 1997; Vol. 2, pp 698−706.
(5) Knözinger, H. In *Handbook of Heterogeneous Catalysis*; Ertl, G., Knözinger, H., Weitkamp, J., Eds.; Wiley-VCH: Weinheim, 1997; Vol. 2, pp 707−732.
(6) Pfeifer, H. In *Handbook of Heterogeneous Catalysis*; Ertl, G., Knözinger, H., Weitkamp, J., Eds.; Wiley-VCH: Weinheim, 1997; Vol. 2, pp 732−740.
(7) Kazansky, V. In *Handbook of Heterogeneous Catalysis*; Ertl, G., Knözinger, H., Weitkamp, J., Eds.; Wiley-VCH: Weinheim, 1997; Vol. 2, pp 740−752.
(8) Guisnet, M. R. *Acc. Chem. Res.* **1990**, *23*, 392.
(9) Hall, K. W. In *Handbook of Heterogeneous Catalysis*; Ertl, G., Knözinger, H., Weitkamp, J., Eds.; Wiley-VCH: Weinheim, 1997; Vol. 2, pp 689−692.
(10) Knözinger, H. *NATO ASI Ser., Ser. C* **1993**, *398*, 267
(11) Zecchina, A.; Lamberti, C.; Bordiga, S. *Catal. Today* **1998**, *41*, 169.
(12) Lavalley, J.-C. *Catal. Today* **1996**, *27*, 377.
(13) Lavalley, J.-C. *Trends Phys. Chem.* **1991**, *2*, 305.
(14) Busca, G. *Phys. Chem. Chem. Phys.* **1999**, *1*, 723.
(15) Busca, G. *Catal. Today* **1998**, *41*, 191.
(16) Zaki, M. I.; Hasan, M. A.; Al-Sagheer, F. A.; Pasupulety, L. *Colloids Surf.* **2001**, *190*, 261.
(17) Morterra, C.; Cerrato, G.; Emanuel, C. *Mater. Chem. Phys.* **1991**, *29*, 447.
(18) Busca, G.; Lorenzelli, V. *Mater. Chem.* **1982**, *7*, 89.
(19) Fouad, N. E.; Thomasson, P.; Knözinger, H. *Appl. Catal., A* **2000**, *194*, 213.
(20) Hasan, M. A.; Zaki, M. I.; Pasupulety, L. *J. Mol. Catal. A* **2002**, *178*, 125.
(21) Coluccia, S.; Baricco, M.; Marchese, L.; Martra, G.; Zecchina, A. *Spectrochim. Acta* **1993**, *49A*, 1289.
(22) Knözinger, H. In *Surface Organometallic Chemistry: Molecular Approaches to Surface Catalysis*, Basset, J.-M., Ed.; Kluwer Academic Publishers: New York, 1988; pp 35−46.
(23) Stark, J. V.; Park, D. G.; Lagadic, I.; Klabunde, K. J. *Chem. Mater.* **1996**, *8*, 1904.
(24) Scarano, D.; Bertarione, S.; Zecchina, A.; Soave, R.; Pacchioni, G. *Phys. Chem. Chem. Phys.* **2002**, *4*, 366.
(25) Yong, Z.; Mata, V. G.; Rodrigues, A. E. *Adsorption* **2001**, *7*, 41.
(26) Mayorga, S. G.; Gaffney, T. R.; Brzozowski, J. R.; Weigel, S. J. *Eur. Pat. Appl.* **2001**, EP 1074297, A2 200110207.
(27) Horiuchi, T.; Hidaka, H.; Fukui, T.; Kubo, Y.; Horio, M.; Suzuki, K.; Mori, T. *Appl. Catal., A* **1998**, *167*, 195.
(28) Busca, G.; Finocchio, E.; Lorenzelli, V.; Ramis, G.; Baldi, M. *Catal. Today* **1999**, *49*, 453.
(29) Finocchio, E.; Willey, R. J.; Busca, G.; Lorenzelli, V. *J. Chem. Soc., Faraday Trans.* **1997**, *93*, 175.
(30) Ulla, M. A.; Spretz, R.; Lombardo, E.; Daniell, W.; Knözinger, H. *Appl. Catal., B* **2001**, *29*, 217.
(31) International Center for Diffraction Data, 12 Campus Boulevard, Newton Square, PA 19073-3273.
(32) Dann, S. E. *Reactions and Characterization of Solids*; The Royal Society of Chemistry: Cambridge, U.K., 2000; pp 64−65.
(33) Mohamed, M. A.; Galwey, A. K. *Thermochim. Acta* **1993**, *217*, 263.
(34) Brunauer, S.; Emmett, P. H.; Teller, E. *J. Am. Chem. Soc.* **1938**, *60*, 309
(35) *CRC Handbook of Chemistry and Physics*, 78th ed.; Lide, D. R., Ed.; CRC Press: New York, 1997−1998.
(36) Peri, J. B.; Hannan, R. B. *J. Phys. Chem.* **1960**, *64*, 1521.
(37) Herzberg, G. *Molecular Spectra and Molecular Structure II*; Van Nostrand: New York, 1962; pp 531−537.
(38) Gregg, S.; Ramasy, J. D. F. *J. Chem. Soc. A* **1970**, *17*, 2784.
(39) Morterra, C.; Ghiotti, G.; Boccuzzi, F.; Coluccia, S. *J. Catal.* **1978**, *51*, 299.
(40) Meyer, A. Y. *Struct. Chem.* **1990**, *1*, 265.
(41) Shen, J.; Tu, M.; Hu, C. *J. Solid State Chem.* **1998**, *137*, 295.
(42) Farragher, A. L. *Adv. Colloid Interface Sci.* **1979**, *11*, 3.
(43) Kus, S.; Otremba, M.; Torz, A.; Taniewski, M. *Appl. Catal., A* **2002**, *230*, 263.
(44) Auroux, A.; Gervasini, A. *J. Phys. Chem.* **1990**, *94*, 6371.
(45) Gervasini, A.; Auroux, A. *J. Therm. Anal.* **1991**, *37*, 1737.
(46) Lahousse, C.; Bachelier, J.; Lavalley, J.-C.; Lauron-Pernot, H.; Le Govic, A.-M. *J. Mol. Catal.* **1994**, *87*, 329.
(47) Zaki, M. I.; Hasan, M. A.; Al-Sagheer, F. A.; Pasupulety, L. *Langmuir* **2000**, *16*, 430.
(48) Zaki, M. I.; Hasan, M. A.; Pasupulety, L. *Langmuir* **2001**, *17*, 768.
(49) Lauron-Pernot, H.; Luck, F.; Popa, J. M. *Appl. Catal.* **1991**, *78*, 213.
(50) Zecchina, A.; Lofthouse, M. G.; Stone, F. S. *J. Chem. Soc., Faraday Trans. 1* **1975**, *71*, 1476.